RESPONSE CHARACTERISTICS OF STRUCTURES SUBJECTED TO BLASTING INDUCED GROUND MOTION

Rajesh Prasad Dhakal[1*] and Tso-Chien Pan[1]

[1]Protective Technology Research Centre, School of Civil and Environmental Engineering, Nanyang Technological University, Block N1, 50 Nanyang Avenue, Singapore 639798

ABSTRACT

This paper presents a conceptual discussion on structural response to ground shocks. Numerical parametric analyses are performed on a simplified linear structural model to investigate the special features of structural response brought by short duration, large amplitude and high frequency excitations, which are the basic characteristics of ground shocks induced by blasting. Nonlinear finite element analyses on a 2-storey RC frame subjected to ground shocks are carried out to qualitatively understand building response to blasting. This study shows that maximum structural response to blasting depends primarily on the amount of impulse, and it generally occurs after the major ground shock has ceased. To capture the maximum response, it is hence necessary to consider additional time duration beyond the major ground shock period in blasting analysis. It is found that the response in the forced-vibration phase includes high frequency vibration modes with small displacement but large acceleration, thus inducing high inertial shear force. However, the free-vibration response is dominated by lower frequency modes with larger displacement but smaller acceleration. Hence, buildings subjected to strong ground shocks might experience a sudden shear failure of its components. Nevertheless, if a building's strength is enough to avoid the sudden shear failure during the major shock, it may be damaged after the ground shock during the free vibration, and the extent of damage depends on the ground shock magnitude.

Keywords: Blasting induced ground motion; impulse; inertial force; shear failure; structural response

[*]Corresponding Author, Fax: (+65)-67910046; E-mail: cdhakal@ntu.edu.sg

1. INTRODUCTION

Storing ordnances in the form of weapon, ammunition, and explosive is an integral part of the defence strategy of each country. Accidental blasting of such storages may cause significant damage to nearby structures. Hence, it is necessary to regulate the construction of residential structures in the vicinity of ammunition arsenals or underground explosive storage facilities. In other words, the closest permissible distance of residential buildings from such magazines, termed as the inhabited building distance (IBD), should be clearly manifested in the specifications. In general, the current practice is based on NATO regulations [1]. Equations proposed in these regulations to recommend IBD were based on analyses and tests conducted between the mid-1950s and the mid-1970s. Obviously, there are uncertainties in the present state-of-the-art, and further research in this field is necessary to identify the areas of technical uncertainties and to determine which of these could lead to significant economic paybacks when the degree of uncertainties is reduced. Due to space, costs and safety issues, extensive experimental investigation of structural response and damage due to blasting is usually not feasible. That is why only a few tests [2-4] have been conducted, and experimental data in this field are scarce. This leaves numerical simulation as an alternative.

In order to estimate IBD reliably, the response of buildings to blasting-induced ground motion (BIGM) must be well understood. It is known that BIGM consists of short duration and large magnitude excitations of high frequency [5]. Due to these unique characteristics, building response to blasting is much different than that to earthquakes. In this pretext, one question remains unanswered: How should the conventional theories of structural dynamics be applied in blasting response prediction? In other words, researches addressing fundamental issues such as the qualitative influences of high frequency, short duration and large magnitude on the structural response to ground shocks are missing. The authors believe that conceptual guidelines based on the interaction between basic structural parameters and ground shock characteristics will be very much helpful in planning and implementing research strategies for further investigations. This paper tries to clarify these basic issues based on the response of a linear single-degree-of-freedom (SDOF) system to BIGM, and also corroborates thus generated conceptual guidelines through nonlinear blasting analysis of a two-storey reinforced concrete (RC) frame.

2. TYPICAL GROUND SHOCK

The magnitude of a BIGM depends on many factors such as quality and quantity of explosives, depth of charge, surrounding soil properties, distance from the source, etc. As an extensive investigation with due consideration to all these parameters is out of scope, BIGM data simulated at different distances for one representative blasting condition [5] are used in this study. Altogether, six ground shocks corresponding to the horizontal and vertical motions simulated at 50, 100 and 150 m surface distance from an underground blasting source of 250 tonnes of TNT are considered. These ground shocks correspond to a one-time explosion of the total charge loaded spherically in an underground chamber that is fully contained. The surrounding rock mass (Granite) was assigned a density of 2650 kg/m^3 and a compressive strength of 148 MPa in the simulation. As a representative case, the acceleration time history of ground shock simulated in horizontal direction at 50 m surface distance and its Fourier transform are shown in Figures 1a and 1b, respectively.

Important parameters such as peak particle velocity (PPV), peak ground acceleration (PGA), and frequency content of all six BIGM records are listed in Table 1. Interestingly, the vertical excitation is found to be significant and non-negligible in comparison with the horizontal one. From Table 1, it is evident that PPV and PGA of BIGMs decrease with the increase in distance but the rate of decrease becomes less prominent as the distance increases. It was also found that the very high frequency components gradually disappear as the distance increases, but the centre of dominant frequency band is only slightly affected within the simulated range. As can be observed in Figure 1 and Table 1, BIGMs have some unique features such as a short duration, large acceleration amplitude and high frequency, which make them distinctly different from common seismic excitations. These characteristics render a BIGM an impulsive jerk rather than a sustained excitation, and a review of dynamic structural response to impulsive loads is helpful in understanding structural response to such ground shocks.

3. IMPULSE RESPONSE: REVIEW

Structural response to impulse can be divided into two phases: the forced-vibration phase (within the impulse duration), and the free-vibration phase (after the impulse has ceased). A structure subjected to impulse usually yields the maximum response in the free-vibration phase. Nevertheless, reliable response prediction in the forced-vibration phase is also important, as the displacement and velocity at the end of this phase serve as the initial conditions for the free-vibration phase. Hereafter, responses of a SDOF system to impulsive ground shocks of four different shapes (sinusoidal, rectangular, symmetric and asymmetric triangular) are computed by solving the Duhamel integral [6]. In computations that follow, 5% damping ratio and PGA of 1000 m/s^2 are assumed for all ground shocks. Responses are computed for three shocks (with duration t_1 equal to 0.2, 0.1 and 0.04 sec), and six SDOF systems (with natural period T equal to 5, 2, 1, 0.5, 0.2 and 0.1 sec) are considered so that the ratio t_1/T ranges between 0.008 and 2.

The displacement response histories of SDOF systems with four different natural periods to a rectangular impulsive ground shock of 0.2 sec duration are shown in Figure 2. For the first two cases (T = 1.0, 0.5 sec), the maximum response occurs in the free-vibration phase, whereas for the third and the fourth cases (T = 0.2, 0.1 sec), response becomes maximum in the forced-vibration phase. Note that the maximum response is significantly smaller when it occurs in the forced-vibration phase. The results indicate that the maximum response does not depend separately on t_1 and T, rather it depends on the ratio t_1/T for all impulse shapes. For symmetrical impulses (sinusoidal, rectangular and triangular), the maximum response lies in the free-vibration phase if t_1/T is less than 0.5, and this critical ratio is 0.37 for asymmetric triangular impulsive load. As the ratio of the effective duration of BIGM to the natural period of most civil engineering structures rarely exceeds the critical ratio, the maximum structural response to blasting usually occurs in the free-vibration phase. This fact advocates for the need to consider a duration longer than the actual ground excitation period in blasting analysis.

As different values of natural period T correspond to different mass and/or stiffness, the absolute displacement responses are not directly comparable. Hence, a generalized parameter called the maximum response factor R_{max}, which is defined as the ratio of the absolute maximum dynamic response to the equivalent static response, is used for comparison among different cases. Here, the equivalent static response is defined as $R_{static} = m \times PGA/k$, where m and k are the oscillator mass and spring stiffness, respectively. For all impulse shapes, the relationships between R_{max} and t_1/T, also called the shock spectra, are drawn in Figure 3a. As expected, the shock spectra corresponding to different impulse shapes are different from one another. Note that R_{max} is proportional to the ratio t_1/T throughout a range where t_1/T is smaller than the critical ratio. For further clarification, R_{max} of the SDOF system with natural period of 1 sec is also plotted in Figure 3b against the normalized total impulse; i.e. the area covered under the

acceleration-time curve. Regardless of the impulse shape, the R_{max}-impulse relationship follows a common path for t_1/T smaller than the critical ratio.

4. EFFECT OF FREQUENCY

Next, special features brought by the dominant high frequency of BIGM in the structural response to blasting are explored. Basically, structural response is a combination of several modes, and each of these modes corresponds to a different frequency. Depending on structural properties and loading characteristics, different modes contribute differently to the overall response. Due to resonance, vibration modes of higher frequency (closer to the dominant frequency of the BIGM) dominate structural response to BIGMs. However, this is true only for the forced-vibration response within the BIGM duration, which is significantly short. On the other hand, vibration modes with a lower frequency (closer to the fundamental frequency of the structure) govern the free-vibration response of a structure to BIGMs. It is, therefore, necessary to understand qualitatively the relative contributions of vibration modes with different frequencies before drawing conclusions.

Hereafter, the response of a linear SDOF system with different natural periods to a typical simulated BIGM is computed to investigate the relative contribution of different modes. To cover all possible vibration modes, an SDOF system is assigned natural frequencies between 0.3 Hz and 300 Hz. To qualitatively represent resonance between the modal frequency and the loading frequency, natural frequency of 188.65 Hz, i.e. equal to the frequency corresponding to the peak of the Fourier spectrum of the applied BIGM, is assigned to one of the SDOF systems. For all computations that follow, damping ratio is assumed to be 1% of the critical. The displacement, velocity and acceleration responses of the SDOF systems with natural frequencies equal to 1 Hz and 100 Hz are shown in Figure 4.

As the spring and damping forces induced depend on the relative displacement and relative velocity, the displacement and velocity responses relative to those of the ground are used in Figure 4. On the other hand, the absolute acceleration responses are plotted, which are responsible for the inertia force induced. As an oscillator with a low fundamental frequency would remain almost stationary during the high-frequency excitations, the absolute acceleration response of the 1 Hz oscillator is negligible during the BIGM period, whereas the relative velocity response shows high frequency components that are attributable to the applied ground velocity. In fact, the acceleration trace would also exhibit significant high-frequency response if the relative values of acceleration were plotted instead of the absolute acceleration. The maximum displacement of the SDOF system with 1 Hz natural frequency occurs in the free-vibration phase, and is significantly larger than the 100 Hz system's maximum displacement response, which occurs in the forced-vibration phase. In contrast, the maximum acceleration of the SDOF system with 100 Hz natural frequency is much larger than that with 1 Hz. The maximum values of displacement, velocity and acceleration of the systems with different natural frequencies are listed in Table 2. As the natural frequency of an SDOF system increases, the maximum displacement decreases. In spite of resonance with the dominant frequency of input BIGM, the maximum displacement of high frequency SDOF system is very small. However, the maximum acceleration increases with an increase in natural frequency.

Although real RC buildings are better represented by a multi-degree-of-freedom (MDOF) system with nonlinear properties, linear response of an SDOF system explains fairly the qualitative features brought by a vibration mode with frequency equal/close to the natural frequency of the SDOF system being considered. These results, therefore, indicate that the maximum acceleration is large and the maximum displacement is small if higher frequency modes are dominant, as in the forced-vibration response to BIGM. Similarly, the maximum acceleration becomes small, and the maximum displacement becomes large if the overall structural response is governed by lower frequency modes, as in the free-vibration response to BIGM. The large acceleration generates a significant inertia force, causing the shear force to increase considerably. On the other hand, the large displacement causes a larger strain that may damage the structure through cracking, yielding, etc. Hence, a structure subjected to an underground blasting would experience a large shear force during the major shock period, and if it sustains the shear force, it would then undergo a significant flexural deformation after the major shock has ceased.

5. CASE STUDY: BLASTING ANALYSIS OF AN RC FRAME

Earlier conclusions were drawn based on linear response of SDOF systems. In order to justify their validity in actual structures, nonlinear dynamic finite element analysis is conducted on a typical two-storey RC building frame subjected to the simulated BIGMs. This numerical investigation is meant to qualitatively investigate the influence of blasting on similar buildings. Though this study is not sufficient to explicitly formulate a general IBD recommendation, it certainly provides a fair idea regarding the

response mechanisms and probable failure types of similar RC building frames when an underground blasting occurs in the vicinity.

5.1 Target Structure

Layout of the representative two-storey RC building frame and its geometrical details are shown in Figure 5. This frame supports one side of a 5 m × 5 m × 150 mm slab resting on the beam in each floor. Density of 25 kN/m^3 is used to compute the self-weight of the RC frame and floor, and live load of 7.5 kN/m^2 is assumed to act on the floors. Following concrete properties are assumed: compressive strength = 30 MPa; tensile strength = 2 MPa; Poisson ratio = 0.2; compressive strain at peak strength = 0.24%; and elastic modulus = 24.8 GPa. Similarly, the properties of steel reinforcement are adopted as follows: yield strength = 410 MPa; ultimate strength = 615 MPa; breaking strain = 5%; and Young modulus = 200 GPa. Shear capacity of the section taken as the sum of the shear contributions from concrete and web reinforcement turns out to be 171.9 kN. Similarly, moment capacity computed according to section analysis is equal to 107.75 kN-m. Assuming the beams to be rigid in axial direction and modelling the frame as a two-degrees of freedom system, frequencies for the first two global horizontal vibration modes are 1.8 Hz and 4.88 Hz, respectively. Similarly, the global natural frequency in the vertical direction is approximately 27 Hz. According to preliminary computations based on a generalized SDOF system assuming both ends pinned, the local transverse vibrations of the beams and columns have fundamental frequencies around 4.3 Hz and 43.3 Hz, respectively.

5.2 Models Used in FE Analysis

A three-dimensional nonlinear finite-element analysis program *Concrete Model in 3D* (COM3) [7] is used for numerical investigation. In COM3, nonlinear dynamic computation is based on the direct integration method. Columns and beams are discretized using frame elements, which are analysed by fibre technique. A fibre may contain either concrete, reinforcing bars, or both concrete and reinforcing bars depending on its position in the cross-section. Response of each fibre is computed using path-dependent cyclic average stress-strain relationships of concrete [8] and reinforcing bars [9]. Moreover, inelastic material mechanisms such as cover concrete spalling [10] and reinforcement buckling [11] are given due consideration in formulating these nonlinear material models. The fibre model for concrete considers the strain rate effect, whereas the effect of strain rate on reinforcing bars, if any, is not taken into account. These models have been experimentally verified at the material and structural levels with sufficient accuracy for static and dynamic analysis of RC members [8].

The two-storey RC frame is discretized into 60 elements (i.e. 10 elements for beams and columns in each storey) and each element consists of 220 parallel fibres. In the analyses, the beam-column joint is modelled as a part of the column. Although the effect of concrete-rebar bond within an element is taken into account in deriving the average stress-strain relationships of the concrete and reinforcement fibres, bond slip between the reinforcing bars and concrete at the joint interfaces is not explicitly considered in the analysis. An equivalent amount of mass is uniformly added throughout the length of the beams to account for the combined live and dead load coming from each floor. Total axial load on each column turns out to be 160 kN, which is around 7.7% of its axial capacity. Fixed supports are provided at the bases of both columns, and simulated BIGMs in the horizontal and vertical directions are applied simultaneously at these supports.

6. NUMERICAL RESULTS

6.1 Response of the Frame to BIGMs Simulated at 50 m

First, the RC frame is subjected to BIGMs simulated at 50 m from the blasting source, and time-history dynamic analysis is conducted. The displacement and acceleration response histories at different points in the frame are obtained from the output. Similarly, variation of the shear force induced at the base of the columns is also extracted. Lateral displacement response histories at different points in the left column are shown in Figure 6. As can be observed, the lateral displacements at different points in the column reach the maximum value almost at the same instant. The maximum displacement at the top of the frame is around 9 mm, which corresponds to about 0.15% average storey-drift. As the displacement histories suggest, high frequency oscillations with small displacement amplitude constitute the responses of all points during the BIGM duration. On the other hand, after the BIGM duration, the roof vibrates in the fundamental global mode, but the response of the first floor level seems to include an additional higher order vibration mode. As expected, the displacement histories of column mid-heights in each storey indicate the presence of local vibration modes that have higher frequencies.

The existence of local vibration modes is also visible in Figure 7a showing the relative maximum lateral displacement profiles of the two columns, which also represent the displaced shapes of the two columns. The dash-and-dot straight line in Figure 7a represents the global mode, and the column displacement from this line is the contribution of local modes, which is more prominent in the second storey. It can be observed that the global lateral displacement is mostly concentrated in the first storey, and relative drift of the second storey is much smaller. Figure 7b shows the maximum transverse acceleration of different points in both columns normalized with respect to the horizontal PGA. It shows that the peak accelerations of the first floor and of the roof are almost equal, and the peak accelerations of intermediate points in the columns are much larger than those at the floor levels. This also corroborates that the columns respond in local modes that have higher frequency than the global mode followed by the floors has.

Figure 8 illustrates the comparison of the induced shear force at the base of the left column with the section shear capacity. In this analysis, shear force induced in the beam may be more severe because of the larger inertia force owing primarily to the floor mass lumped in the beam. In actual response, the mass is distributed throughout the floor area, and the beam shear force would not be as detrimental. However, shear force induced in the columns is not influenced by the distribution pattern of the dead and live loads. The comparison in Figure 8 shows that the induced base shear is distinctly less than the shear capacity, i.e. 172 kN. Nevertheless, the maximum shear force, in this case, occurred in the left column just below the first floor. The maximum shear force induced at that location was equal to 165 kN, still slightly less than the predicted capacity. Note that the induced shear force becomes maximum during the forced-vibration phase, and the shear capacity corresponding to a higher loading rate is not necessarily equal to the one predicted earlier. During a high frequency excitation, the contribution of concrete may increase due to the increase in material strength, but the stirrups may not contribute as the shear cracks are expected to be perpendicular to the column axis rather than inclined at 45^o, as assumed in the truss analogy. Consequently, the overall shear capacity may decrease slightly.

To qualitatively indicate the extent of damage, the extreme strains of the outermost fibres in the beam and column cross-sections near the joints are shown in Figure 9. Strain histories of the extreme fibres at the most critical location in the beam and the column are also included in the figure. As can be seen, strain induced after the major shock period is larger than that induced during the major shock period. The maximum strains at some locations are larger than yielding strain of the reinforcing bars ($\cong$2000 $\mu\varepsilon$), especially at the beam-ends and columns just below the roof level. Hence, formation of plastic hinges at these locations cannot be ruled out. As strains in all locations exceed cracking strain of concrete ($\cong$150 $\mu\varepsilon$), cracks are expected to appear throughout the frame.

The response of the frame along the vertical direction is not discussed in detail because its magnitude is subjected to change depending on the distribution of the floor loads. However, the qualitative nature of the vertical response remains the same. Vertical displacement patterns of the beams in the two floors are found to resemble with each other. Downward displacement is maximum at the centre of the beam but negligible at the joints. Moreover, the peak vertical accelerations at the beam-ends are significantly higher than those at the intermediate points along the beam length. Both of these observations indicate that the joints follow the global vertical mode that has higher natural frequency due to the large axial stiffness of columns, but the beam vibrates in its local mode, which has a comparatively lower natural frequency.

6.2 Response to Weaker BIGMs

Next, the same RC frame is subjected to the BIGMs simulated at 100 m and 150 m from the blasting source, respectively. Note that these BIGMs may also represent ground shocks at the same distance (i.e. 50 m) but from an underground blasting of a smaller scale. Though not shown in detail, responses in both cases are found to be qualitatively similar to those due to the 50 m BIGMs. As expected, the maximum shear force induced in the column is much less than the section shear capacity, and the possibility of shear failure does not exist at all. Lateral displacements are smaller, e.g. average storey-drift due to the 100 m BIGMs is less than 0.1%. As in the previous case, high frequency vibration modes could be noticed in the response histories. Figures 10a and 10b show respectively the maximum displacement profiles of the columns and the extreme strains in the outermost fibres at some critical locations when the frame is subjected to the 100 m BIGMs. In spite of the small storey-drift, strains are found to be non-negligible, especially at the beam-ends and at the columns just below the roof level. Localized damages are expected at the beam-ends in the first storey, and some sporadic cracks are expected in other parts as well. When the frame is subjected to the 150 m BIGMs, numerical results show that the maximum strains at almost all locations are less than the yielding strain. Hence, the frame does

not experience much damage although a few cracks may appear at some locations. These numerical results indicate that the typical two-storey RC building frame is moderately damaged when an underground blasting of the simulated scale takes place at a distance of 50 m, but it can bear without much damage the same or a smaller explosion at a distance larger than 100 m.

6.3 Response to Stronger BIGMs

Next, the same RC frame is subjected to two times the magnitude of ground shock simulated for 50 m distance from the blasting source. The magnified ground motions may represent either one or both of the following conditions: (i) ground shock at a closer distance from the blasting source, and (ii) ground shock induced by a larger amount of explosive. As shown in Figure 11a, the maximum lateral displacement at the roof level is around 2.0 cm (i.e. 0.33% average storey-drift). The maximum tensile and compressive fibre strains at some locations of the frame are illustrated in Figure 11b. As expected, the maximum strains are much larger than those in the previous cases, and the frame might experience severe damage. The shear force induced at the base of the left column is compared with the section shear capacity in Figure 12. It can be observed that the maximum base shear force induced during the major shock period is larger than the section shear capacity. Considering that the maximum shear force in the column just below the second storey is even higher, shear failure is highly likely to take place. The frame may collapse due to a sudden shear failure during the major shock before experiencing a severe damage in the free-vibration phase. Note that the frame did not show signs of shear failure due to BIGMs at 50 m although a substantial structural damage was anticipated in the free-vibration phase.

6.4 Qualitative Damage Attenuation

Based on these numerical results, overall safety of the RC building frame located at various distances from the blasting source can be qualitatively assessed. Figure 13 illustrates schematically the qualitative relationship between the extent of damage of the frame and the distance between the frame and the blasting source. The solid line (curve 1) in Figure 13 represents the damage attenuation curve plotted based on the analysed cases, and it corresponds to the simulated explosive quantity (indicated as Q_s in Figure 13). As indicated by the predicted frame response to BIGMs at 150 m, safety of the frame far from the blasting source is guaranteed. At a very close distance from the blasting source, the frame may undergo a sudden shear failure of some of its components during the forced-vibration phase as in the case of the magnified BIGMs. A frame located outside the shear failure zone (indicated as D_{sh} in Figure 13) can safely survive the forced-vibration phase, but may still experience structural damage in the free-vibration phase, as indicated by the frame response to BIGMs at 50 m and 100 m. The structural damage might be severe if the frame is inside the critical damage zone (indicated as D_{cr} in Figure 13), and moderate or small if it is outside the critical damage zone.

Based on the analysed cases, qualitative damage attenuation curves for different amounts of explosive (indicated as Q in Figure 13) are extrapolated and shown as three dashed lines in Figure 13. Curve 2 corresponds to a larger explosion, and curves 3 and 4 correspond to explosions smaller than that for which the BIGMs were simulated. In general, two damage mechanisms can be identified, namely shear collapse in the forced-vibration phase and structural damage in the free-vibration phase. As found earlier, the possibility of shear failure and the extent of structural damage due to a BIGM are governed by the scale of applied impulse. Hence, the frontiers of shear failure zone and critical structural damage zone depend primarily on the amount of explosive. The ranges of shear failure zone and critical damage zone are wider for a larger explosion, such as the one represented by curve 2. Similarly, these ranges become smaller for smaller explosions. It is also possible that both of these zones may not exist at all if the quantity of explosive is very small as represented by curve 4. In such cases, the explosion is too small to fail or to critically damage a structure regardless of its distance from the blasting source. For a moderate scale of explosion represented by curve 3, a narrow critical damage zone may exist but the shear failure zone may not exist.

7. FUTURE RESEARCH DIRECTIONS

Note that the damage attenuation curves shown in Figure 13 and the subsequent discussions are for the representative frame adopted in the numerical analysis. Although the trend of damage attenuation for other structures is qualitatively similar, the ranges of the shear failure zone and the critical structural damage zone would be different because these ranges also depend on the structural toughness apart from the explosion scale. For example, an explosion may be hazardous for a weak building and, at the same time, harmless for a stronger building.

Hence, future studies should be planned to explore simple but general methods to compute the structural toughness and an appropriate BIGM parameter representing the blasting scale. These two parameters can be mutually compared to check if the structure undergoes shear failure during the major shock. Research is also deemed necessary to establish empirical relationships between a ground shock impulse and structural response parameters at the end of the shock, which would serve as the initial conditions to compute the ensuing free-vibration response. This would relieve the designers from conducting the time-consuming time history dynamic analysis.

8. CONCLUSIONS

Fundamental concepts of structural dynamics are employed to explain the characteristics of structural response to underground blasting. BIGM has some special characteristics such as high frequency, large amplitude and short duration. Parametric studies based on the response of an SDOF system to BIGMs were carried out to highlight the effect of these special features on various structural response parameters. Due to the impulsive nature of BIGMs, the maximum structural response usually occurs after the major ground shock, and is proportional to the total impulse applied. Hence, analyses aimed to predict structural response to blasting should cover a time domain much longer than the ground shock duration, and response computations performed only within the major ground shock duration will underestimate the maximum structural response.

The forced-vibration response to a BIGM is dominated by higher frequency vibration modes, whereas the free-vibration response is mainly governed by lower frequency vibration modes. The higher frequency modes cause a smaller displacement but a larger acceleration, thus causing a high shear force in the forced-vibration phase. Hence for structures closer to a large-scale underground blasting source, a sudden shear failure may take place during the forced-vibration phase due to the excessive input energy or impulse. On the other hand, the lower frequency modes cause a larger displacement and a smaller acceleration, thus increasing the possibility of structural damage in the free-vibration phase. The existence of these two damage mechanisms are verified with blasting time-history analyses of a representative building frame subjected to various BIGMs. Based on the results, conceptual damage attenuation curves for the representative frame are presented for different amount of explosives. These curves provide a clear insight on the vulnerability of buildings when subjected to an underground blasting at different distances.

ACKNOWLEDGEMENTS

The authors gratefully acknowledge the financial support from the Defense Science and Technology Agency, Singapore.

REFERENCES

[1] North Atlantic Treaty Organization. Manual on NATO safety principles for the storage of ammunition and explosives. Document AC/258-D/258. Brussels, 1999.
[2] Skjeltorp A. Underground ammunition storages: Model tests to investigate external safety distances. Fortifikatorisk Notat 36/67. Norwegian Defence Construction Service. Oslo, 1967.
[3] Murrell DW and Joachim CE. The 1996 Singapore ground shock test. Waterways Experiment Station. Department of Army. Vicksburg, 1996.
[4] Zhao J, Wu YK, Cai JG, Chen SG and Zhao YH. Small–scale ground shock tests at the Mandai quarry. Technical Report to the Lands and Estates Organization, Ministry of Defence. Singapore, 1997.
[5] Ma G, Hao H and Zhou YX. Modelling of wave propagation induced by underground explosion. Computers and Geotechnics 1998; 22(3-4):283-303.
[6] Clough RW and Penzien J. Dynamics of Structures. McGraw-Hill, 1993.
[7] Maekawa K, Irawan P and Okamura K. Three-dimensional constitutive laws of reinforced concrete. Proceedings of the International Conference on Applied Concrete Mechanics APCOM. Seoul (South Korea): 1996. p. 1471-1476.
[8] Okamura H and Maekawa K. Nonlinear Analysis and Constitutive Models of Reinforced Concrete. Tokyo: Gihodo Publication, 1991.
[9] Dhakal RP and Maekawa K. Path-dependent cyclic stress-strain relationship of reinforcing bar including buckling. Engineering Structures 2002; 24(11):1383-1396.

[10] Dhakal RP and Maekawa K. Reinforcement stability and fracture of cover concrete in reinforced concrete members. Journal of Structural Engineering. ASCE 2002; 128(10):1253-1262.
[11] Dhakal RP and Maekawa K. Modeling for postyield buckling of reinforcement. Journal of Structural Engineering. ASCE 2002; 128(9):1139-1147.

Table 1. Characteristics of simulated BIGMs

Distance, m (Direction)	PPV, m/s	PGA, m/s^2	Frequency range, Hz	Dominant band and frequency at peak, Hz
50 (Horizontal)	0.98	1220.19	<1200	95-260 (188.65)
100 (Horizontal)	0.58	428.89	<800	50-225 (105.72)
150 (Horizontal)	0.43	343.16	<500	50-235 (103.65)
50 (Vertical)	0.87	1234.61	<700	120-285 (209.61)
100 (Vertical)	0.29	340.87	<600	30-400 (148.00)
150 (Vertical)	0.24	241.87	<500	40-320 (128.53)

Table 2. Effect of natural frequency on maximum response

Maximum Response	Natural frequency of SDOF system, Hz					
	0.3	1.0	10.0	100.0	188.7	300.0
Displacement, mm	414.2	119.4	9.2	3.0	3.1	0.7
Velocity, m/s	1.2	1.2	1.1	2.0	3.7	1.2
Acceleration, m/s^2	1.5	4.7	36.3	1176.4	4328.2	2331.0

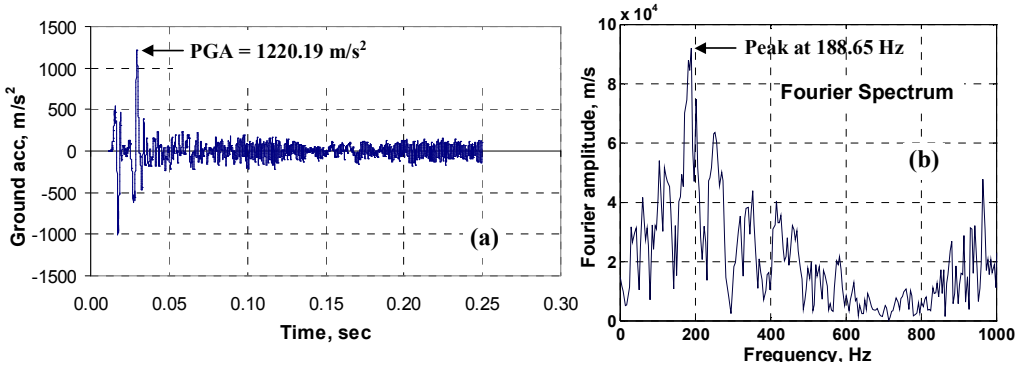
PGA = 1220.19 m/s²
Ground acc, m/s²
Time, sec
(a)
Peak at 188.65 Hz
Fourier Spectrum
(b)
Fourier amplitude, m/s
x 10⁴
Frequency, Hz

Figure 1

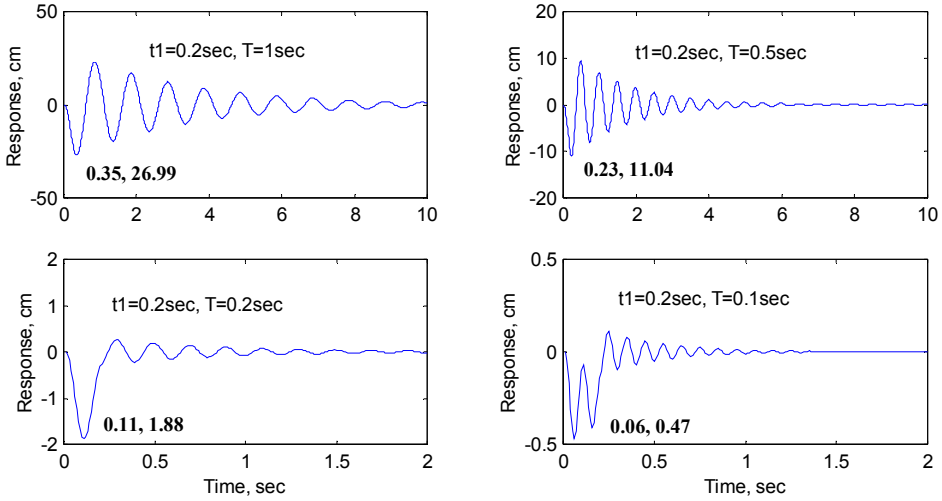
t1=0.2sec, T=1sec
0.35, 26.99
t1=0.2sec, T=0.5sec
0.23, 11.04
t1=0.2sec, T=0.2sec
0.11, 1.88
t1=0.2sec, T=0.1sec
0.06, 0.47
Response, cm
Time, sec

Figure 2

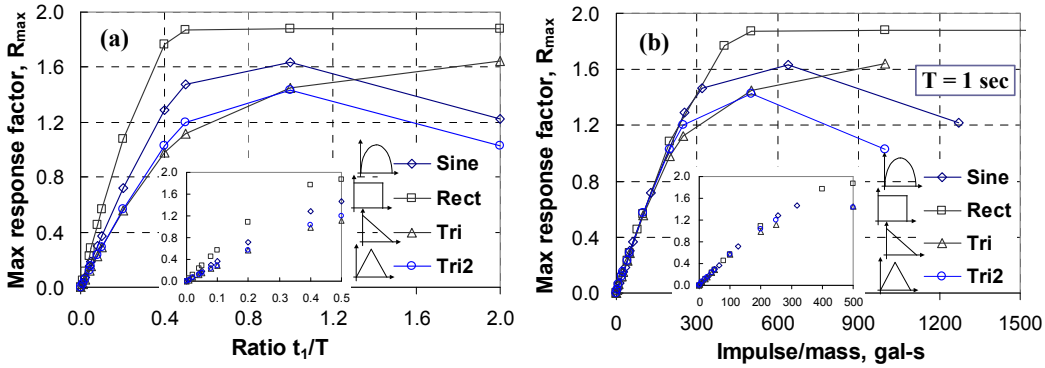
(a)
Max response factor, R_{max}
Ratio t_1/T
Sine
Rect
Tri
Tri2
(b)
T = 1 sec
Impulse/mass, gal-s

Figure 3

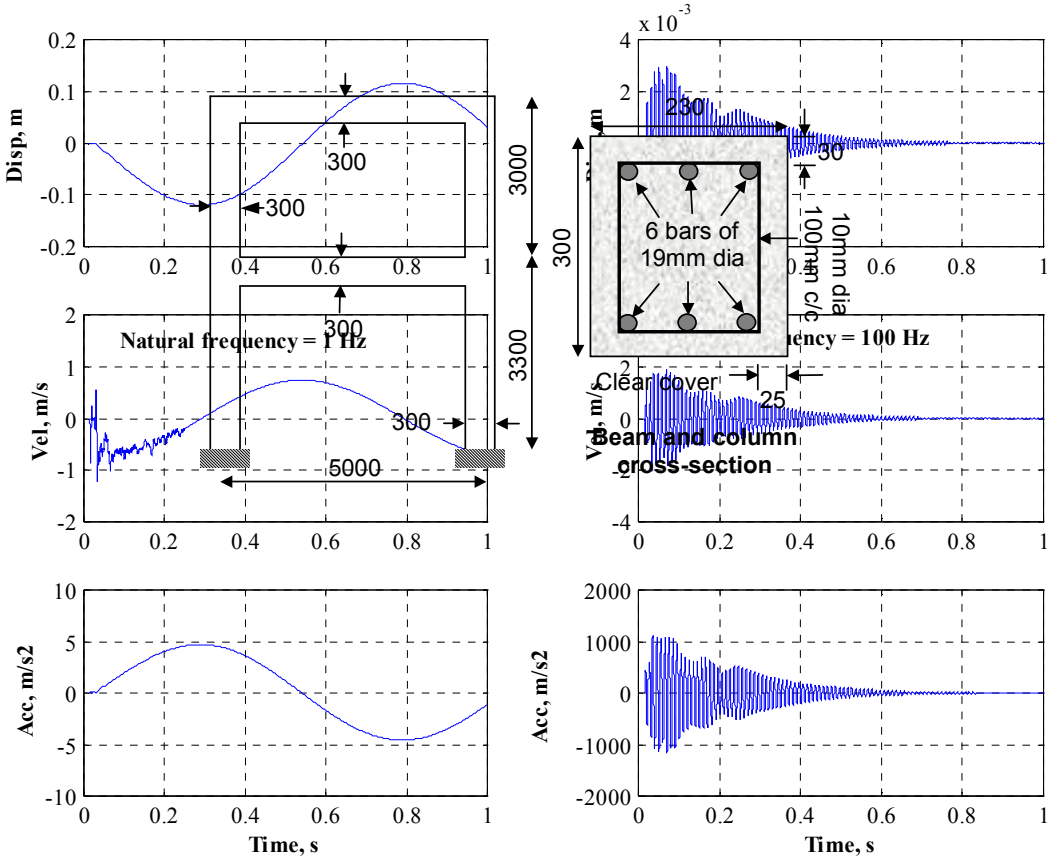

Figure 4

Figure 5

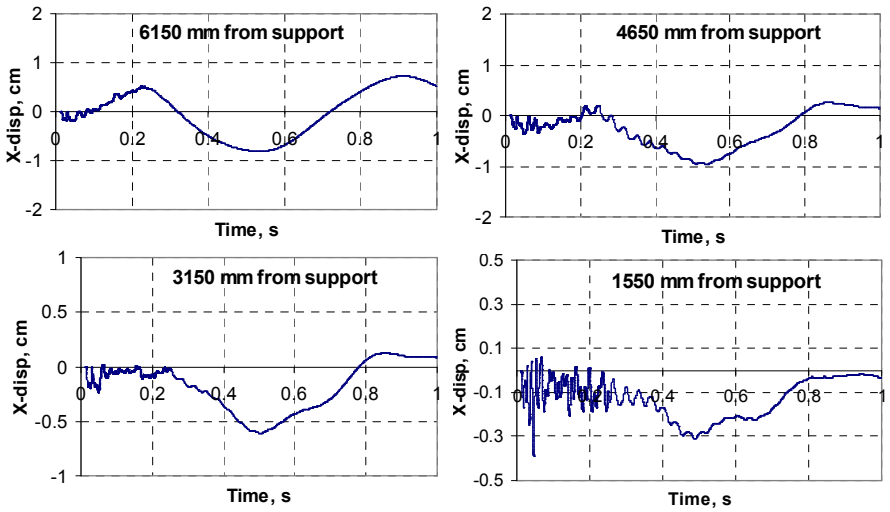
6150 mm from support
4650 mm from support
3150 mm from support
1550 mm from support
X-disp, cm
Time, s

Figure 6

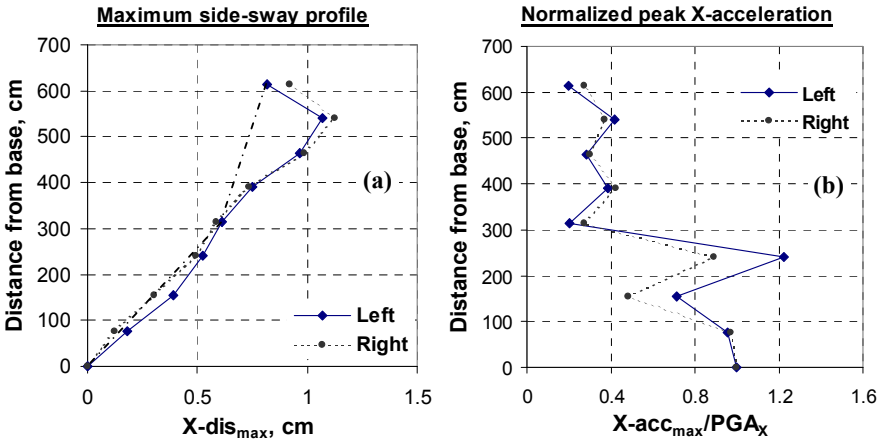
Maximum side-sway profile
Distance from base, cm
700
600
500
400
300
200
100
0
0
0.5
1
1.5
X-dis$_{max}$, cm
(a)
Left
Right
Normalized peak X-acceleration
Distance from base, cm
0
0.4
0.8
1.2
1.6
X-acc$_{max}$/PGA$_X$
(b)
Left
Right

Figure 7

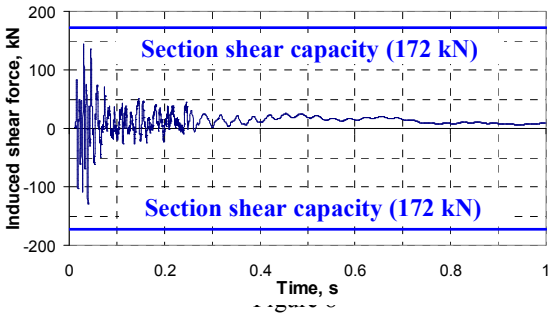
Section shear capacity (172 kN)
Section shear capacity (172 kN)
Induced shear force, kN
Time, s
200
100
0
-100
-200
0
0.2
0.4
0.6
0.8
1

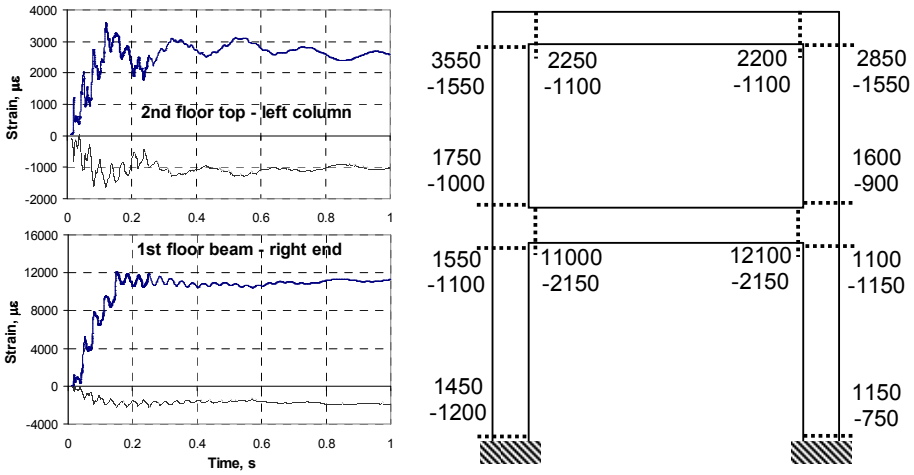
Strain, με
2nd floor top - left column
1st floor beam - right end
Time, s
3550
-1550
2250
-1100
2200
-1100
2850
-1550
1750
-1000
1600
-900
1550
-1100
11000
-2150
12100
-2150
1100
-1150
1450
-1200
1150
-750

Figure 9

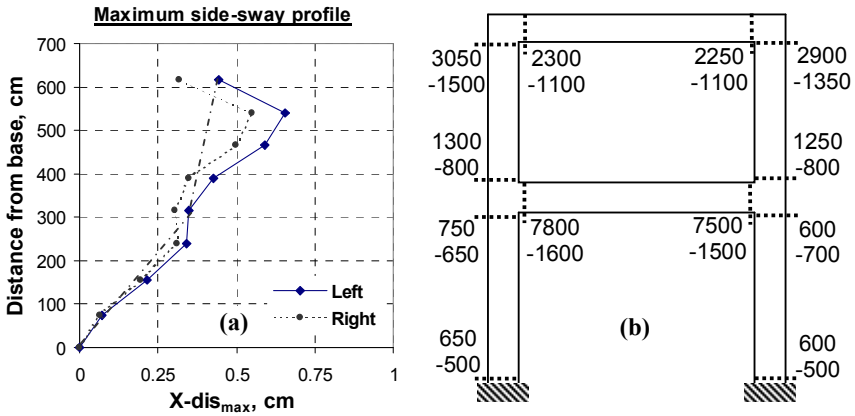
Maximum side-sway profile
Distance from base, cm
X-dis$_{max}$, cm
Left
Right
(a)
(b)
3050
-1500
2300
-1100
2250
-1100
2900
-1350
1300
-800
1250
-800
750
-650
7800
-1600
7500
-1500
600
-700
650
-500
600
-500

Figure 10

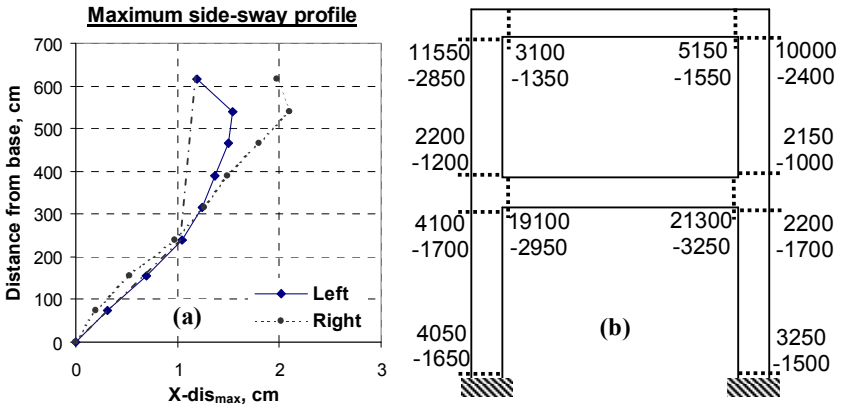
Maximum side-sway profile
Distance from base, cm
700
600
500
400
300
200
100
0
0
1
2
3
X-dis$_{max}$, cm
Left
Right
(a)
11550
-2850
3100
-1350
5150
-1550
10000
-2400
2200
-1200
2150
-1000
4100
-1700
19100
-2950
21300
-3250
2200
-1700
4050
-1650
(b)
3250
-1500

Figure 11

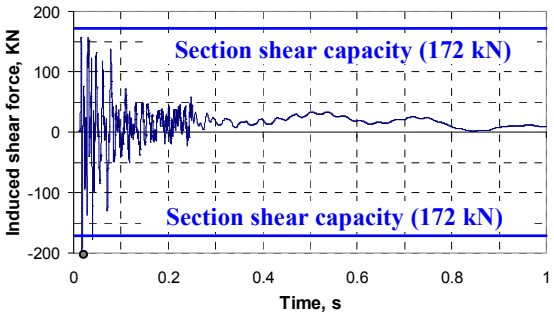
Section shear capacity (172 kN)
Section shear capacity (172 kN)
Induced shear force, KN
Time, s
200
100
0
-100
-200
0
0.2
0.4
0.6
0.8
1

Figure 12

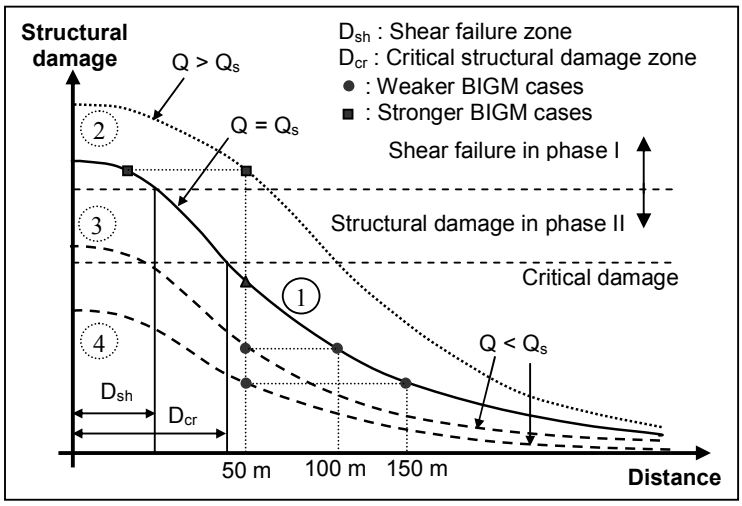
Structural damage
Q > Qs
Q = Qs
Dsh : Shear failure zone
Dcr : Critical structural damage zone
: Weaker BIGM cases
: Stronger BIGM cases
Shear failure in phase I
Structural damage in phase II
Critical damage
Q < Qs
2
3
1
4
Dsh
Dcr
50 m
100 m
150 m
Distance

Figure 13